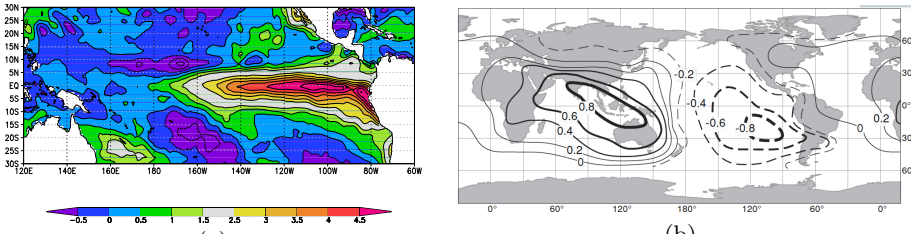

(a) (b)

FIGURE 18. *(a) Sea-surface temperature anomaly field (with respect to the 1982-2010 mean) of December, 1997, at the height of the 1997/1998 El Niño. Data from NOAA, see http://www.emc.ncep.noaa.gov/research/cmb/sst_analysis/. (b) Correlations of sea level pressure anomalies over the Tropic Pacific, illustrating the Southern Oscillation.*

5. El Niño/Southern Oscillation

5.1. *Phenomena*

About once every four years, the sea surface temperature in the equatorial eastern Pacific is a few degrees higher than normal (Philander 1990). Near the South American coast, this warming of the ocean water is usually at its maximum around Christmas. Long ago, Peruvian fishermen called it El Niño , the Spanish phrase for the "Christ Child".

During the last decades, El Niño has been observed in unprecedented detail thanks to the implementation of the TAO/TRITON array and the launch of satellite-borne instruments (McPhaden & coauthors 1998). The relevant quantities to characterize the state in the equatorial ocean and atmosphere are sea level pressure, sea surface temperature (SST), sea level height, surface wind and ocean sub-surface temperature.

The annual mean state of the equatorial Pacific sea-surface temperature is characterized by the zonal contrast between the western Pacific "warm pool" and the "cold tongue" in the eastern Pacific. The mean temperature in the eastern Pacific is approximately 23°C, with seasonal excursions of about 3°C. What makes El Niño unique among other interesting phenomena of natural climate variability is that it has both a well-defined spatial pattern and a relatively well-defined time scale. The pattern of the sea-surface temperature anomaly for December 1997 is plotted in Fig. 18a and shows a large area where the SST is larger than average. Changes in the tropical atmospheric circulation are strongly connected to changes in sea-surface temperature . Hence, there are strong correlations between surface pressure anomalies, as shown in Fig. 18b.

An index of this sea-surface temperature anomaly pattern is the NINO3 index, defined as the sea-surface temperature anomaly averaged over the region 5°S –5°N, 150°W–90°W. In the time series (blue curve in Fig. 19a), the high NINO3 periods are known as El Niño's and the low NINO3 periods as La Niña's. There is no clear-cut distinction between El Niño's, La Niña's, and normal periods, rather the system exhibits continuous fluctuations of varying strengths and durations with an average period of about 4 years (blue curve in Fig. 19b).

The red curve in Fig. 19a is the normalized pressure difference between Tahiti (Eastern Pacific region) and Darwin; this index is referred to as the Southern Oscillation Index (SOI). It measures the variations in the tropical surface winds, dominated by the trade winds. When the SOI is negative (positive) , the pressure in Tahiti is relatively low (high) with respect to that in Darwin and hence the trade winds are weakened (strengthened). The anti-correlation of the NINO3 index and the SOI is obvious from Fig. 19a and the spectrum of the SOI in Fig. 19b also shows a similar broad peak as the NINO3 index

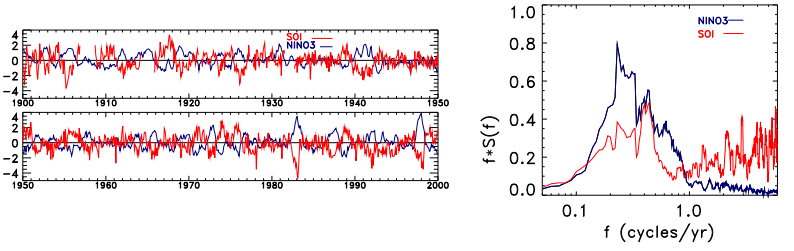

(a) (b)

FIGURE 19. *(a) Time series of the NINO3 index (dark) and SOI (light) over the years 1900-2000. (b) Spectrum of the NINO3 index (dark) and SOI (light) in (a), where on the vertical axis the product of frequency f and the spectral power $S(f)$ is plotted (figure based on Dijkstra & Burgers (2002)).*

(centered at about 4 year). As El Niño and the Southern Oscillation are one phenomenon, it is referred to as the ENSO phenomenon.

There are relations between the seasonal cycle, the spatial sea-surface temperature pattern of the annual-mean state and the El Niño variability. Large sea-surface temperature anomalies often occur within the cold tongue region. In addition, El Niño is to some extent phase-locked to the seasonal cycle as most El Niño's and La Niña's peak around December. The root mean square of the NINO3 index is almost twice as large in December than in April.

When one considers the spectrum of the NINO3 index (Fig. 19b), also energy is found at lower frequencies, in particular in the decadal-to-interdecadal range (Jiang *et al.* 1995; Zhang *et al.* 1997; Fedorov & Philander 2000). The strength of El Niño before the mid-1970s appears to be smaller than that after this period; this transition is sometimes referred to as the 'Pacific climate shift' (Trenberth 1997). According to NCEP data, the standard deviation of the SOI (NINO3) for 1951-1975 is 1.64 (0.81), to be compared for 1976-2000 where it is 1.84 (1.00). The spatial pattern of these (multi)decadal changes is fairly similar to that of the interannual variability, but the sea-surface temperature anomalies at the eastern side of the basin extend from the equator to midlatitudes (Zhang *et al.* 1997).

5.2. *The Zebiak & Cane model*

To capture the oscillatory behavior of ENSO dynamically, a coupled atmosphere-ocean model is required, which admits feedbacks between perturbations to the equatorial easterlies, the thermocline depth, and equatorial SSTs, and as such allows the spontaneous growth of anomalies. We shall also see that oceanic wave dynamics are important to the development and decay of El Niño's, and so necessary in a minimal model of ENSO.

5.2.1. *Model formulation*

Zebiak & Cane (1987), hereon ZC, consider a $1\frac{1}{2}$-layer reduced gravity ocean (depicted in Figure 20) below a constant-depth mixed layer of temperature T, which feels a temperature-dependent wind stress

$$\tau^x = \tau^x_{\text{ext}} + \mu\mathcal{A}(T - T_0), \tag{5.1}$$

for some atmospheric operator $\mathcal{A}$, and coupling parameter μ (with $\mu = 0$ corresponding to the entirely uncoupled case, and $\mu = 1$ describing "normal" coupling).

The reduced gravity ocean model equations for the horizontal velocities (u, v) and

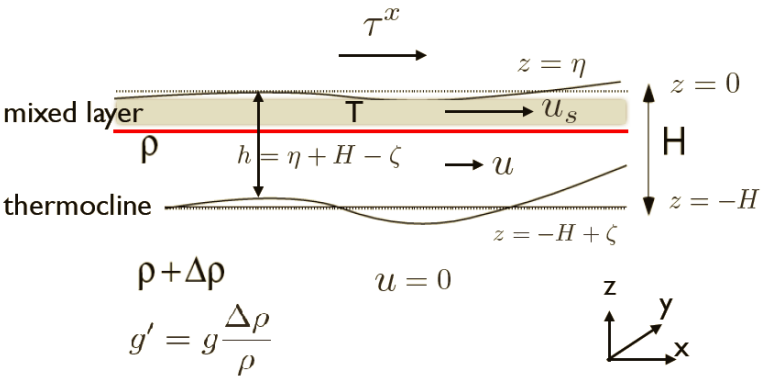

FIGURE 20. *The ocean component of the ZC model. A thermocline of density ρ overlies a denser stationary layer of density $\rho + \Delta\rho$. The ocean feels atmospheric wind stress and temperature through constant depth mixed layer of temperature T.*

thermocline depth h are

$$\frac{\partial u_1}{\partial t} - \beta_0 y v_1 = -g' \frac{\partial h}{\partial x} + \frac{\tau^x}{\rho H}, \tag{5.2a}$$

$$\beta_0 y u_1 = -g' \frac{\partial h}{\partial y}, \tag{5.2b}$$

$$\frac{\partial h}{\partial t} = -H\left(\frac{\partial u_1}{\partial x} + \frac{\partial v_1}{\partial y}\right), \tag{5.2c}$$

with boundary conditions

$$x = 0 \ : \int_{-\infty}^{\infty} u_1(y)dy = 0, \tag{5.3a}$$

$$x = L \quad : u_1 = 0, \tag{5.3b}$$

$$y \to \pm\infty : u_1,\ v_1,\ h, \text{ bounded.} \tag{5.3c}$$

The evolution of the mixed layer temperature T is governed by an advection-diffusion equation with relaxation back to the radiation equilibrium temperature T_0 as follows

$$\frac{\partial T}{\partial t} + u_1\frac{\partial T}{\partial x} + v_1\frac{\partial T}{\partial y} + w_1\mathcal{H}(w_1)\frac{T - T_s(h)}{H} + \alpha_T(T - T_0) - \kappa_H\nabla^2 T = 0, \tag{5.4}$$

where $\mathcal{H}$ is the Heaviside function (needed because the mixed layer temperature is only affected by net upwelling). In addition, the subsurface temperature $T_s(h)$ is a monotonically increase function of h and κ_H is a horizontal diffusion coefficient. The boundary conditions for the mixed layer temperature are

$$x = 0,\ L \quad : \frac{\partial T}{\partial x} = 0, \tag{5.5a}$$

$$y \to \pm\infty : T \text{ bounded.} \tag{5.5b}$$

5.2.2. *Equatorial wave dynamics in the ZC model*

Consider free waves with $\tau^x = 0$, corresponding to no wind stress input, and no coupling with the mixed layer temperature field T. Let $u = \hat{u}(y)e^{i(kx-\sigma t)}$ and define $v = \hat{v}(y)e^{i(kx-\sigma t)}$ and $h = H + \hat{h}(y)e^{i(kx-\sigma t)}$ similarly. Then

$$-i\sigma\hat{u} - \beta_0 y\hat{v} = -ikg'\hat{h}, \tag{5.6a}$$

$$\beta_0 y\hat{u} = -g'\hat{h}', \tag{5.6b}$$

$$-i\sigma\hat{h} + H(ik\hat{u} + \hat{v}') = 0. \tag{5.6c}$$

Solutions with $\hat{v} = 0$ are determined from

$$-\sigma\hat{u} = -g'k\hat{h}, \tag{5.7a}$$
$$-\sigma\hat{h} + Hk\hat{u} \quad = 0, \tag{5.7b}$$
$$\tag{5.7c}$$

which has a non-zero solution only if

$$\sigma^2 = k^2 g' H, \tag{5.8}$$

and so

$$\frac{\sigma}{k} = \pm\sqrt{g'H} \equiv \pm c_0. \tag{5.9}$$

We can also solve for $\hat{h}$ and $\hat{u}$, since

$$\beta_0 y\hat{u} = \frac{\beta_0 y g' k\hat{h}}{\sigma} = -g'\hat{h}', \tag{5.10}$$

and so

$$\hat{h}(y) = \hat{h}(0)\exp\left[-\frac{\beta_0 k}{2\sigma}y^2\right] \equiv \hat{h}(0)\exp\left[-\frac{1}{2}\left(\frac{y}{\lambda_0}\right)^2\right], \tag{5.11}$$

where $\lambda_0 = \sqrt{c_0/\beta_0}$ is the Rossby deformation radius. Note that for $\hat{h}(y)$ to be bounded as $y \to \pm\infty$ we have to set $\sigma/k = +c_0$. These eastward propagating waves are called equatorial Kelvin waves.

The general case $\hat{v} \neq 0$ can also be solved by using the Hermite polynomials H_n, giving

$$\hat{u}_j(y) = \tfrac{1}{2\sqrt{2}}\left(\tfrac{\psi_{j+1}(y)}{\sqrt{j+1}} - \tfrac{\psi_{j-1}(y)}{\sqrt{j}}\right), \tag{5.12a}$$
$$\hat{h}_j(y) = \tfrac{1}{2\sqrt{2}}\left(\tfrac{\psi_{j+1}(y)}{\sqrt{j+1}} + \tfrac{\psi_{j-1}(y)}{\sqrt{j}}\right), \tag{5.12b}$$
$$\hat{v}_j(y) \qquad\quad = \psi_j(y), \tag{5.12c}$$

where

$$\psi_j(y) = \frac{H_j(y/\lambda_0)\exp[-(y/\lambda_0)^2/2]}{(2^j j!\pi^{1/2})^{1/2}}, \tag{5.13}$$

and the corresponding phase speeds are

$$c_j = -\frac{c_0}{2j+1}. \tag{5.14}$$

These westward propagating waves are called equatorial Rossby waves.

5.2.3. *Coupled feedbacks in the ZC model*

To explore the feedbacks possible in the full model, consider a perturbation (denoted by hats) to some steady state (denoted by overbars) of the simplified temperature equation

$$\frac{\partial T}{\partial t} = -w\frac{T - T_s(h)}{H}. \tag{5.15}$$

Linearizing about the steady state, this becomes

$$\frac{\partial \hat{T}}{\partial t} = -\hat{w}\frac{\bar{T} - T_s(\bar{h})}{H} - \bar{w}\frac{\hat{T} - T_s'(\bar{h})\hat{h}}{H}. \tag{5.16}$$

Now it can be seen that if there is a warm anomaly in the mixed layer (i.e. $\hat{T} > 0$) giving rise to a deepening of the thermocline (i.e. $\hat{h} > 0$), the second term on the right

of equation 5.16 will be positive, leading to more warming. This positive f eedback is known as the *thermocline feedback*.

Similarly, from the first term on the right of equation 5.16, it can be deduced that a positive temperature anomaly, associated with a reduction in upwelling ($\hat{w} < 0$), will likewise enhance the positive temperature anomaly, acting as a positive feedback. This is called the *upwelling feedback*. An analogous treatment of the zonal advection terms of the temperature equation

$$\frac{\partial T}{\partial t} = -u\frac{\partial T}{\partial x} \tag{5.17}$$

yields linearized equation

$$\frac{\partial \hat{T}}{\partial t} = -\bar{u}\frac{\partial \hat{T}}{\partial x} - \hat{u}\frac{\partial \bar{T}}{\partial x}. \tag{5.18}$$

Now a positive temperature anomaly will produce a zonal velocity anomaly $\hat{u}$ that acts to enhance this anomaly by the advection of the mean temperature field $\bar{T}$. This is the *zonal advection feedback*.

5.3. *Hopf bifurcation in the ZC model*

The zonal wind stress τ^x is decomposed into an external and a coupled contribution (Van der Vaart *et al.* 2000):

$$\tau^x = \tau^x_{ext} + \tau^x_c, \tag{5.19}$$

The coupled part of the wind stress is assumed to be proportional to the zonal wind field u_a, i.e., $\tau^x_c = \rho H \gamma_\tau U$, with γ_τ a constant coefficient. The velocity field U is determined from an equivalent barotropic atmospheric model given by (Matsuno 1966; Gill 1980)

$$\frac{\partial U}{\partial t} - \beta_0 y V - \frac{\partial \Theta}{\partial x} + a_M U = 0 \tag{5.20a}$$

$$\frac{\partial V}{\partial t} + \beta_0 y U - \frac{\partial \Theta}{\partial y} + a_M V = 0 \tag{5.20b}$$

$$\frac{\partial \Theta}{\partial t} - c_a^2\left(\frac{\partial U}{\partial x} + \frac{\partial V}{\partial y}\right) + a_M \Theta = Q \tag{5.20c}$$

where (U, V) are the low level winds, Θ the geopotential height (with dimension m^2/s^2), a_M is a damping coefficient and c_a is the phase speed of the first baroclinic Kelvin wave in the atmosphere. The flow is forced by a representation of the adiabatic heating term Q (having dimension m^2/s^3) given by

$$Q = \alpha_T (T - T_0) \tag{5.21}$$

The external wind stress τ^x_{ext} does not depend on the coupled feedbacks within the basin and can be thought of to represent the easterly stress component due the Hadley circulation and it is assumed constant in the zonal direction (Dijkstra & Neelin 1995). In the meridional direction the external wind stress is assumed to be symmetric with respect to the equator, having the form (Van der Vaart *et al.* 2000)

$$\tau^x_{ext} = -\tau_0 e^{[-\frac{1}{2}(\frac{y}{L_a})^2]}, \tag{5.22}$$

where τ_0 is a typical amplitude of the external wind stress and L_a is the atmospheric Rossby deformation radius.

In order to obtain the proper climatology of the present-day Pacific together with realistic ENSO variability, the standard parameter values as in Table 3 are used. The coupling parameter μ_0 is a dimensionless product of the dimensional parameters and is

TABLE 3. *Values of dimensional parameters used in the ZC model.*

L	$= 1.5 \times 10^7$	[m]	c_0	$= 2$	[m/s]
c_a	$= 30$	[m/s]	H	$= 200$	[m]
H_1	$= 50$	[m]	H_2	$= 150$	[m]
τ_0	$= 0.01$	[Pa]	T_{s0}	$= 23.0$	[°C]
a_m	$= 1.3 \times 10^{-8}$	[s^{-1}]	T_0	$= 30.0$	[°C]
a_s	$= 5.0 \times 10^{-6}$	[s^{-1}]	$\hat{H}$	$= 40$	[m]
a_T	$= 9.25 \times 10^{-8}$	[s^{-1}]	h_0	$= 20$	[m]
A_m	$= 2.5 \times 10^{-6}$	[s^{-1}]	β_0	$= 2.2 \times 10^{-11}$	[$(ms)^{-1}$]
g'	$= 0.02$	[ms^{-2}]	L_a	$= 1.5 \times 10^6$	[m]
α_T	$= 5.4 \times 10^{-3}$	[$m^2 s^{-3} K^{-1}$]	γ_τ	$= 6.5 \times 10^{-6}$	[s^{-1}]

given by

$$\mu_0 = \mu \frac{\alpha_T \gamma_\tau \Delta T L^2}{c_o^2 c_a^2} \tag{5.23}$$

where ΔT is a typical SST difference over the basin, here taken as $\Delta T = 1°C$. The dimensionless parameter μ is used below to control the strength of the coupling.

To solve the model equations numerically, variables are expanded into spectral basis functions, with Chebychev polynomials in zonal direction and Hermite functions in meridional direction Van der Vaart *et al.* (2000). The solutions are then obtained by a collocation method with N_x collocation point in the zonal direction and N_y in the meridional direction. In the deterministic ZC model, with the parameters as in Table 1, a Hopf bifurcation occurs at $\mu = \mu_c = 3.0$ Van der Vaart *et al.* (2000). When the coupling strength is smaller than μ_c, for example $\mu = 2.7$, the system is in the subcritical regime where it exhibits a damped ENSO oscillation when no noise is present. This is shown in the behavior of the NINO3.4 index (red curve) in Fig. 21a. When the coupling strength is increased to just above the critical value ($\mu = 3.02 > \mu_c$), the system will enter the supercritical regime where the NINO3.4 index displays an interannual oscillation (red curve in Fig. 21c) and the spectrum shows a peak at about 4 years (red curve in Fig. 21d). When an additive (white) noise forcing is added to the deterministic zonal wind stress (Eq. 5.22), the response of the ZC model is shown as the black curves in Fig. 21a-b (subcritical) and 21c-d (supercritical). In the subcritical regime, the noise forcing is necessary to excite the ENSO variability, while in the supercritical regime, the noise forcing simply causes a higher amplitude of ENSO variability (Roulston & Neelin 2000).

5.4. *Physical mechanisms for ENSO*

We have seen from the ZC model that with idealized ocean-atmosphere coupling and oceanic wave dynamics it is possible to find oscillatory solutions in certain parts of parameter space that resemble ENSO in amplitude and period. Below we heuristically describe two mechanisms that might give rise to such oscillatory behavior.

Consider a positive temperature anomaly at the equator in the Pacific ocean, which corresponds to a positive SSH anomaly on-equator, with compensatory negative SSH anomalies off-equator to the north and south. We have seen that such a signal may propagate eastwards as an equatorial Kelvin wave on the equator, which may be interpreted as the eastward propagating and growth of an El Niño. Meanwhile, the off-equator signal will propagate westward as a Rossby wave and, on reaching the westerward basin boundary, may be reflected as an equatorial Kelvin wave. This reflected wave signal has

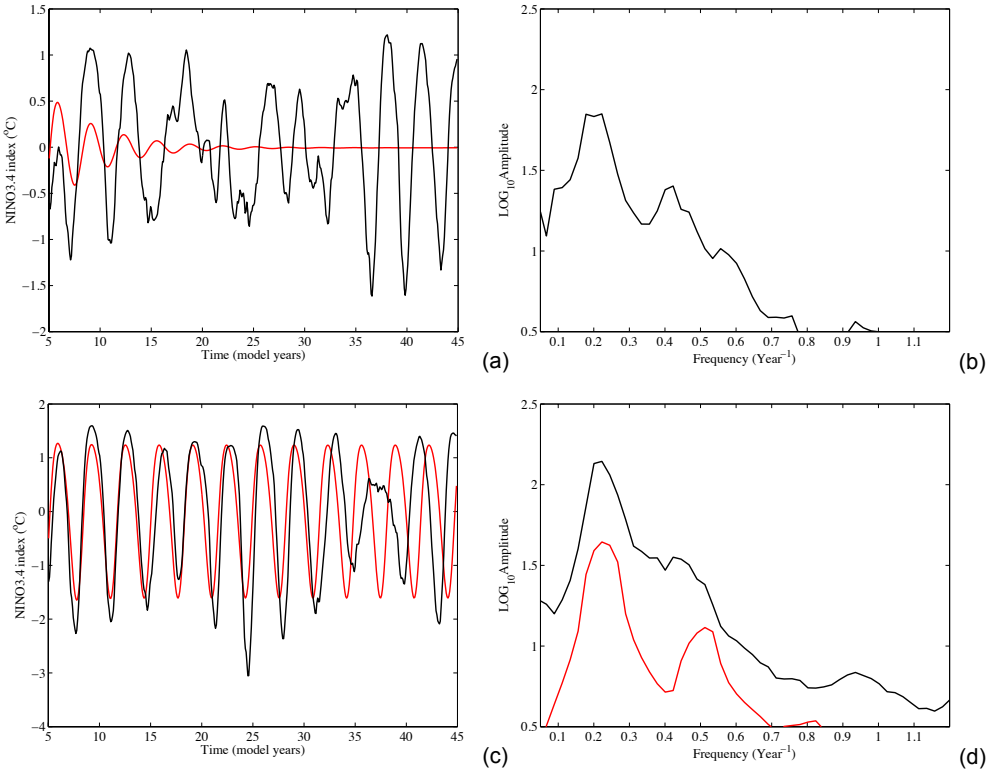

FIGURE 21. *The response of the Zebiak and Cane (ZC) model. Red curves are for the deterministic model and black curves are for the stochastic model with red noise wind-stress forcing. (a) The NINO3.4 index at a coupling strength* $\mu = 2.7$*, (b) The amplitude spectrum for (a), (c) Same as (a) but at* $\mu = 3.02$*, (d) The amplitude spectrum for (c).*

the possibility of interfering with and killing the original positive temperature anomaly, ending the El Niño. Whilst this delayed oscillator mechanism of El Niño undoubtedly influences ENSO dynamics, a consideration of the timescales involved (from the Kelvin and Rossby wave speeds) does not explain the observed ENSO period of four to seven years (Schopf & Suarez 1988; Battisti 1988).

An alternative mechanism that produces longer timescale variability comes from considering the overall basin adjustment. A positive SST anomaly in the eastern Pacific will produce a westerly wind stress anomaly. The wind stress acts to change the thermocline slope, piling up water and so depressing the thermocline in the east, whilst shoaling the thermocline in the west. Such a perturbation to the thermocline slope will enhance the SST perturbation, acting as a positive feedback. As the positive temperature anomaly strengthens, there is a divergent transport of heat off-equator by the ocean, which shoals the thermocline, suppressing the SST anomaly and so reducing the westerly wind anomaly. The shoaling of the thermocline eventually carries the system into the opposite phase, with a negative SST anomaly in the east, and so an easterly wind stress anomaly. This causes the convergent transport of heat to the equator, resulting in the 'recharge' of the ocean heat content there. As such, this mechanism is known as the *recharge oscillator* view of ENSO (Jin 1997). This process is shown schematically in Fig. 22.

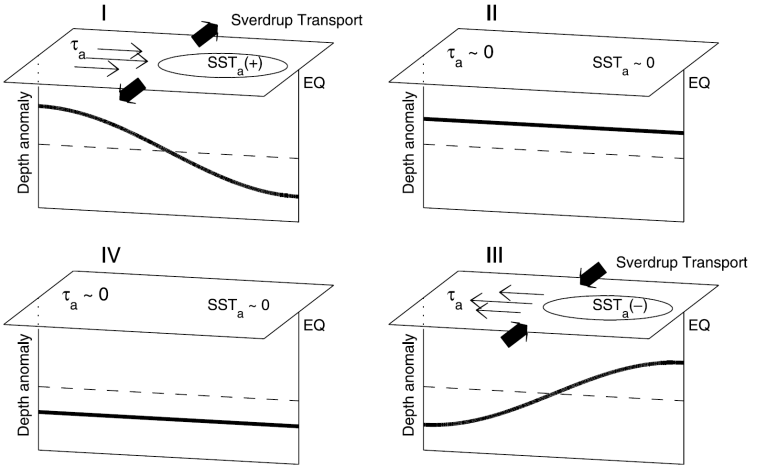

FIGURE 22. *A schematic of the stages of the recharge oscillator mechanism for ENSO.*

5.5. *The irregularity of ENSO*

So far we have seen that the oscillatory behavior of El Nino Southern Oscillation (ENSO) mechanism was related to the saturation of a unstable mode above the threshold of a Hopf bifurcation, corresponding to a given critical coupling strength between the atmosphere and the ocean. However, this does not explain the irregularity, for example in the NINO3 time series. Two views exist on this irregularity: in one view it arises through nonlinear interactions between ENSO and the seasonal cycle, in another it arises solely through atmospheric noise.

5.5.1. *Deterministic chaos*

An interesting point in the record of the ENSO signal is the signature of some mean seasonal cycle. For the western tropical Pacific ocean, negative anomalies in the records of zonal winds occur around April, whereas positive anomalies occur around December. Furthermore, sea surface temperature (SST) anomalies are observed at the same periods: positive SST anomalies are associated with negative zonal wind anomalies, and negative SST anomalies are associated with positive zonal wind anomalies. It is important to note that ENSO events and the seasonal cycle are sensitive to the same environmental factors such as wind forcing and the ocean circulation. ENSO's non-linear interaction with the seasonal cycle is characterized by a tendency to synchrony in periodic, subharmonic oscillation.

An idealized model to understand the interaction of an external and internal frequency is the circle map

$$x_{n+1} = x_n + \Omega - \frac{K}{2\pi}\sin(2\pi x) \quad (mod\ 1) \tag{5.24}$$

In order to illustrate the tendency for phase-locking we pick up a constant driving frequency Ω and a starting point x_0. The result of the iterations displaying the interaction between anomalies and the driving cycle is obtained by displaying the computed winding number W, given by

$$W = \lim_{n\to\infty} \frac{x_n - x_0}{n} \tag{5.25}$$

in the (Ω, x) plane, for all the described Ω. As we increase the parameter K in the non-linear forcing, an increasing number of 'windows' are opening and widening in the (Ω, x)

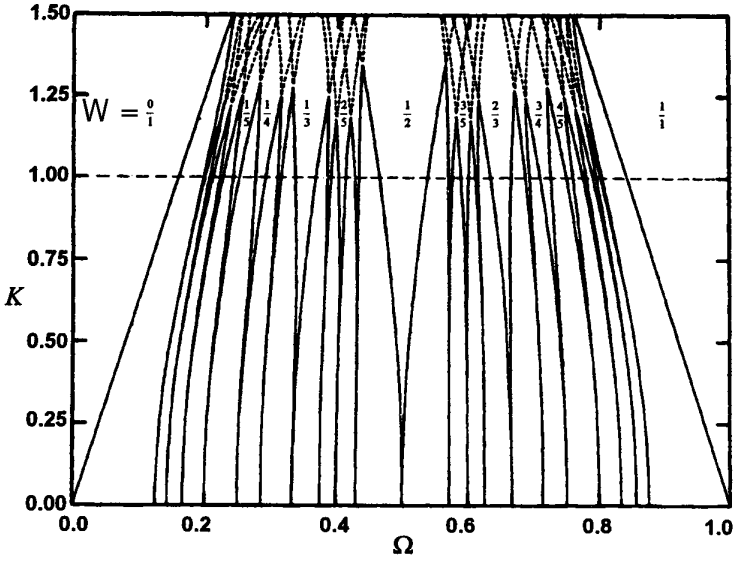

FIGURE 23. *Plot of regions of rational rotation number in the $\Omega - K$ plane displaying the Arnold tongues (Bak* et al. *(1985)) for the circle map.*

space, the so-called Arnold' tongues. These windows are the orbital periods (Fig. 23) of limit circles encountered in the iterative process, and correspond to rational multiples of the driving frequency Ω onto which the system is locking. The frequency ratio of the model to the driving frequency describe a "devil's staircase" as the number and width of frequency-locked steps (corresponding to the windows) increases infinitely. Above $K = 1$, chaotic behavior (sensitive dependence on initial conditions) is found due to the overlap of Arnold' tongues. This route to chaotic behavior is called the quasi-periodicity route.

In the Zebiak-Cane model the interaction between the seasonal cycle and the Hopf bifurcation oscillatory frequency has been studied in the parameter plane spanned by the atmospheric/oceanic coupling strength parameter μ and the upwelling feedback parameter δ leading to a so-called 'Devil's terrace' (Fig. 24). As the coupling strength is increased, both the amplitude and the time scale of the oscillations are enhanced. By varying the parameters μ and δ, Zebiak-Cane model predicts frequency locked ENSO events (e.g. 3 ENSO's in 10 years) in some regions in parameters space and chaotic behavior in others.

5.5.2. *Effects of noise*

Unresolved fast and short scales can be integrated into ENSO models by adding noise. As an example, the westerly wind bursts (WWB) events are characterized by velocities above 7 m s^{-1}, with a typical duration of a few days. These unresolved processes are known to trigger the propagation of perturbations in the form of equatorial Kelvin and Rossby waves. The correlation between this events can be verified in using a singular value decomposition analysis of the SST-Wind covariance matrix. The response of Zebiak-Cane model to white noise was shown in Fig. 21 for both subcritical and supercritical regimes. A remarkable result is that wind-stress noise can trigger a response even before the critical point for the Hopf bifurcation is reached, that is, while still in the subcritical regime.

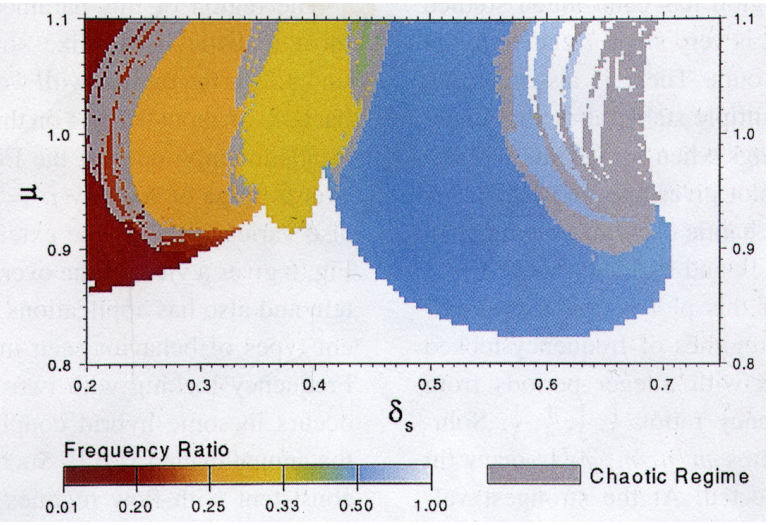

FIGURE 24. *The Devil's terrace as computed in Jin* et al. *(1996). Colors indicate the frequency locked regimes, with chaotic regimes in between. Along a section for fixed μ, a Devil's staircase appears.*

To study the effect of noise in more detail, we consider the following SDE system

$$dX_t = (\lambda X_t - \omega Y_t - X_t(X_t^2 + Y_t^2))dt + \sigma dW_1, \tag{5.26a}$$
$$dY_t = (\lambda Y_t + \omega X_t - Y_t(X_t^2 + Y_t^2))dt + \sigma dW_2. \tag{5.26b}$$

where dW_1 and dW_2 are independent Wiener processes.

In polar coordinates ($r = \sqrt{X^2 + Y^2}$ and $\theta = \arctan \frac{X}{Y}$), we get for the stochastic part (using Ito's formula for change of variables and omitting the subscript t):

$$\begin{aligned} dR =& \frac{\partial r}{\partial x} dX + \frac{\partial r}{\partial y} dY + \frac{1}{2}\Big(\frac{\partial^2 r}{\partial x^2}(dX)^2 + \frac{\partial^2 r}{\partial y^2}(dY)^2\Big) + ... \\ =& \frac{X}{r}\sigma dW_1 + \frac{Y}{r}\sigma dW_2 + \frac{1}{2}\Big(\frac{Y^2}{r^3}(\sigma)^2 + \frac{X^2}{r^3}(\sigma)^2\Big)dt + ... \\ =& \underbrace{\sigma(\cos\theta dW_1 + \sin\theta dW_2)}_{\text{noise term}} + \underbrace{\frac{\sigma^2}{2r}dt}_{\text{additional drift term}}, \\ d\theta =& -\frac{y}{r^2}\sigma dW_1 + \frac{x}{r^2}\sigma dW_2 + \frac{1}{2}\Big(\frac{2XY}{r^4}(\sigma)^2 - \frac{2XY}{r^4}(\sigma)^2\Big)dt + ... \\ =& \underbrace{\sigma\Big(\frac{\cos\theta}{r}dW_2 - \frac{\sin\theta}{r}dW_1\Big)}_{\text{additional drift term}}. \end{aligned}$$

and hence (5.26) is transformed into

$$dR = (\lambda r - r^3 + \frac{\sigma^2}{2r})dt + \sigma(\cos\theta dW_1 + \sin\theta dW_2), \tag{5.27a}$$
$$d\theta = \sigma\Big(\frac{\cos\theta}{r}dW_2 - \frac{\sin\theta}{r}dW_1\Big) + \omega dt. \tag{5.27b}$$

The stationary probability density function is determined from the Fokker-Planck

equation associated with the stochastic system above. We obtain for the drift

$$\mathbf{f} = \begin{pmatrix} \lambda r - r^3 + \frac{\sigma^2}{2r} \\ \omega \end{pmatrix}$$

and for the diffusion matrix

$$\mathbf{g} = \sigma \begin{pmatrix} \cos\theta & \sin\theta \\ -\frac{\sin\theta}{r} & \frac{\cos\theta}{r} \end{pmatrix}$$

The diffusion operator $\mathbf{D}$ is then

$$\mathbf{D} = \mathbf{g}\mathbf{g}^T = \sigma^2 \begin{pmatrix} 1 & 0 \\ 0 & \frac{1}{r^2} \end{pmatrix}$$

and the Fokker-Planck equation

$$\frac{\partial p}{\partial t} = -\frac{\partial[(\lambda r - r^3 + \frac{\sigma^2}{2r})p]}{\partial r} - \frac{\partial(\omega p)}{\partial \theta} + \frac{\sigma^2}{2}\left(\frac{\partial^2 p}{\partial^2 r} + \frac{1}{r^2}\frac{\partial^2 p}{\partial^2 \theta}\right) \tag{5.28}$$

We look for a stationary radially symmetric density function $p_s(r)$ which satisfies then

$$0 = -\big((\lambda r - r^3 + \frac{\sigma^2}{2r})p_s\big)' + \frac{\sigma^2}{2}p_s''$$

which can be easily solved through

$$\frac{p_s'}{p_s} = -\frac{2}{\sigma^2}\lambda r - 2\frac{r^3}{\sigma^2} + \frac{1}{r}$$

$$\ln p_s = -\frac{\lambda}{\sigma^2}r^2 - \frac{r^4}{2\sigma^2} + \ln r$$

and finally we obtain

$$p_s(r) = N \exp\left(\frac{\lambda r^2}{\sigma^2} - \frac{r^4}{2\sigma^2}\right) \tag{5.29}$$

where N is again a normalization constant.